Effect of Pb-underpotential deposition on anodic dissolution and passivation of pure Fe and Fe-Ni alloys in acidic perchlorate solution

Masahiro Seo [1] · Hiroki Habazaki [1] · Takenori Nakayama [2]

[1] Division of Materials Chemistry, Faculty of Engineering, Hokkaido University, 0608628 Sapporo, Japan

[2] Materials Research Laboratory, Kobe Steel Ltd., 6512271 Kobe, Japan

Corresponding Author: Masahiro Seo

masaseo@eng.hokudai.ac.jp

Abstract The potentio-dynamic polarization curves of pure Fe, Fe-30 Ni and Fe-70 Ni alloys in acidic perchlorate solutions (pH 1.9) without and with 10^{-3} M Pb^{2+} were measured to investigate the effect of Pb-underpotential deposition (Pb-UPD) on anodic dissolution and passivation in relation to Pb-induced stress corrosion cracking (Pb-SCC) of Ni base alloys. The addition of 10^{-3} M Pb^{2+} shifts the open circuit potentials of pure Fe and Fe-Ni alloys toward noble direction to inhibit the anodic dissolution and promote the passivation, which results from Pb-UPD on substrate metals. The electro-desorption of Pb proceeds with anodic potential sweep and the anodic dissolution is enhanced when the surface coverage of Pb is reduced to a critical level. Tafel slopes (b^+ = 8.5 ~ 15 mV decade^{-1}) of anodic dissolution for pure Fe and Fe-Ni alloys in the presence of Pb^{2+} are significantly low as compared with those (b^+ = 34 ~ 40 mV decade^{-1}) in the absence of Pb^{2+}, which reflects on the rapid enhancement in surface reactivity as a result of electro-desorption of Pb. It is found that the potential region in which anodic dissolution is inhibited by Pb-UPD is located within the potential window of Pb-UPD estimated from the differences in work-function between substrate metals and Pb.

Keywords Pure Fe · Fe-Ni alloy · Underpotential deposition (UPD) of Pb · Anodic dissolution · Passivation

Introduction

It has been reported that a trace amount of Pb species in solutions induces stress corrosion cracking of high nickel alloys such as alloy 600 and 800 used as tubing materials for nuclear steam generators in pressurized water reactors [1-4]. The main features of Pb-induced stress corrosion cracking (Pb-SCC) have been reviewed by Staehle [1,2]. The roles of soluble Pb species in Pb-SCC and its mechanism, however, have not been sufficiently clarified because of complicated solution chemistry in the operation conditions at high pressure and high temperature.

Several researchers [5-8] have investigated the effect of soluble Pb species on polarization behaviors of pure Ni and / or Ni base alloys at low temperature below 100 ^{o}C. Radhakrishnan et al. [7] have found that an addition of Pb^{2+} inhibits the anodic dissolution of pure Ni in 0.1 M $HClO_4$ solution, while in acetic acid/ sodium acetate buffer solution (pH 3.5) the anodic dissolution is enhanced by Pb^{2+} and have suggested that the effect of Pb^{2+} on anodic dissolution of Ni is associated with underpotential deposition (UPD) of elemental Pb on Ni.

The term "UPD" is applied to the electro-adsorption of metal ions (M^{z+}) on foreign metal substrate (M`) at potentials more noble than the equilibrium potential of M^{z+} / M electrode [9,10]. As reviewed by Herrero et al. [11], there are many studies of UPD on well-defined single-crystal noble metal substrates such as Ag, Au and Pt with relation to the enhancement of electro-catalytic activity due to UPD. In contrast there are comparatively few studies of the effect of UPD on metal corrosion [12-14]. Besides, most of the corrosion studies could not show any clear evidences of UPD.

Our recent studies [8,15] by combined spectroscopic / electrochemical measurements have succeeded in obtaining the quantitative relation between Pb-UPD and corrosion of Ni in acidic perchlorate solution at room temperature: 1) the presence of Pb species adsorbed on Ni was confirmed by X-ray photoelectron spectroscopy (XPS) and glow discharge-optical emission spectroscopy (GDOES), 2) adsorbed Pb species suppress the anodic dissolution of Ni, 3) the anodic dissolution of Ni, however, is activated by electro-desorption of Pb, and 4) in-situ X-ray absorption spectroscopy (XAS) has revealed that the Pb species adsorbed on Ni is metallic.

According to Kolb et al. [9,10], UPD can take place when ions of a lower work-function metal are in contact with a higher work-function substrate metal and the potential window of UPD is determined by the difference in work-function between adsorbed metal and substrate metal. The work-function of polycrystalline Pb (Φ_{Pb} = 4.25 eV) [16] is lower than that of polycrystalline Ni (Φ_{Ni} = 5.15 eV) [16], supporting strongly that Pb-UPD proceeds on Ni. Fe as well as Cr are the indispensable components of high nickel alloys, e.g., alloy 800 contains 44 mass% Fe and 21 mass% Cr. The work-function of polycrystalline Fe (Φ_{Fe} = 4.5 eV) is higher by 0.25 eV than that of polycrystalline Pb (Φ_{Pb} = 4.25 eV) [16], suggesting that Pb-UPD proceeds on Fe to some extent. In fact, it has been reported that Pb^{2+} inhibits the anodic dissolution of Fe in perchlorate and sulfate solutions at potentials more noble than the equilibrium potential of Pb^{2+}/ Pb system, which is ascribed to Pb-UPD on Fe [14].

It is known that the anodic behavior of Fe-Ni binary alloy in 5 % H_2SO_4 is intermediate to the anodic behavior of pure Fe and Ni [17] and the anodic dissolution current peak decreases with increasing Ni content [18]. The potential window of Pb-UPD on Fe-Ni alloy would expand with increasing Ni content

because the work-function of Ni is higher than that of Fe. It is expected that Pb-UPD behaviors on Fe-Ni alloys depend sensitively on the alloy composition to influence the anodic dissolution. In this paper, the effect of Pb-UPD on anodic dissolution and passivation of pure Fe and Fe-Ni alloys in acidic perchlorate solution was investigated in relation to Pb-SCC.

Experimental

The specimens used for experiments were pure Fe plate (purity> 99.9 %) with a size of 10 x 10 x 1.0 mm, Fe-30 Ni and Fe-70 Ni alloy plates with a size of 10 x 10 x 1.5 mm. The chemical compositions of the specimens are listed in Table 1. The Fe specimen was annealed in vacuum at 873 K for 30 min and cooled in air, while the Fe-Ni alloy specimens were annealed in vacuum at 1123 K for 30 min and quenched into water to fix in γ-phase. The Fe and Fe-Ni alloy specimens were mechanically polished on wet SiC papers down to # 1500 and then with α-alumina abrasives (0.3 μm), washed with distilled water, washed with acetone using an ultrasonic technique, finally dried with air.

The electrolytes used for experiments were 0.1 M $NaClO_4$ + 10^{-2} M $HClO_4$ solutions (pH 1.9) with and without 10^{-3} M Pb^{2+}. Lead was added as PbO to give the specified concentration of Pb^{2+} in solution. The electrolytes were prepared from guaranteed reagent grade chemicals (Kanto Chemical Co. Inc.) with ultrapure water supplied through a super Millipore Milli Q filter system. Before introduction in the electrochemical cell, the electrolytes were deaerated with ultrapure argon gas in solution reservoirs. The deaeration of the electrolytes was also maintained during electrochemical measurements by flowing ultrapure argon gas into the cell.

The electrochemical cell with a solution volume of about 100 cm^3 was made from glassware. A platinum plate was used as the counter electrode. The electrode potential was measured with an Ag /AgCl electrode in a saturated KCl solution and converted to the scale of standard hydrogen electrode (SHE). The electrochemical measurements were performed at room temperature (25 ±1 ^oC). The open-circuit potential, E_{ocp} of each specimen in solution without or with 10^{-3} M Pb^{2+} was measured until it attains a steady state (after 15 min). After E_{ocp} attained a steady state, the potentio-dynamic polarization of each specimen was performed at a potential sweep rate of 1.0 mV s^{-1} from E_{ocp} to anodic direction until an anodic-limit potential, $E_{a,l}$, or from E_{ocp} to cathodic direction until a cathodic-limit potential, $E_{c,l}$, then to anodic direction. The cathodic-limit potential, $E_{c,l}$, was set to the potential less noble than the equilibrium potential (10^{-3} M Pb^{2+}/ Pb), E_{eq} = - 0.215 V (SHE) in order to discriminate electrochemically between UPD and bulk deposition processes of Pb.

Results and discussion

Polarization behavior of pure Fe

Figure 1a shows the anodic polarization curves of pure Fe obtained with a potential sweep (1.0 mV s^{-1})

from E_{ocp} to $E_{a,l}$ in deaerated 0.1 M $NaClO_4$ + 10^{-2} M $HClO_4$ solutions without and with 10^{-3} M Pb^{2+}. $E_{a,l}$ was set at the potential corresponding to an anodic current density of 8 mA cm^{-2}. The steady state values of E_{ocp} in solutions without and with 10^{-3} M Pb^{2+} are - 0.337 ± 0.004 V and - 0.206 ± 0.008 V (SHE), respectively. E_{ocp} shifts toward noble direction by 0.13 V due to addition of 10^{-3} M Pb^{2+} indicating that Pb^{2+} inhibits the anodic dissolution of Fe. The inhibition of anodic dissolution of Fe due to addition of Pb^{2+} is consistent with previous report [14]. E_{ocp} in solution without 10^{-3} M Pb^{2+} is less noble by 0.122 V than the equilibrium potential of 10^{-3} M Pb^{2+}/ Pb, E_{eq} = - 0.215 V (SHE) and is located within the potential region of Pb-bulk deposition. In contrast, E_{ocp} in solution with 10^{-3} M Pb^{2+} is slightly more noble than E_{eq} = - 0.215 V (SHE) and is located on the border of Pb-UPD potential region. It is remarked that in solution with 10^{-3} M Pb^{2+}, a short induction period of $\tau \approx 10 \sim 30$ mV appears prior to the rapid increase in anodic dissolution current. The potential of rapid increase in anodic dissolution current, $E_{i,a}$ = - 0.185 ± 0.002 V is independent of fluctuation in E_{ocp}. In the absence of Pb^{2+}, E_{ocp} (i.e., corrosion potential) of pure Fe is determined by coupled reactions of anodic dissolution and hydrogen evolution. In the presence of Pb^{2+}, the electro-adsorption of Pb would participate in determination of E_{ocp}.

In general, UPD takes place up to a full monolayer of adsorbed metal atoms at the equilibrium potential of M^{z+}/ M system [11]. Thus, it is deduced that the Fe surface at E_{ocp} in solution with 10^{-3} M Pb^{2+} is covered with an adsorption amount of Pb nearly equal to a monolayer and the active dissolution sites of Fe are blocked with adsorbed Pb to induce the suppression of anodic dissolution. The anodic potential sweep from E_{ocp}, however, induces Pb electro-desorption from Fe surface. The anodic dissolution of Fe is activated as the Pb electro-desorption proceeds. The appearance of short induction period may be associated with initiation of Pb electro-desorption and $E_{i,a}$ is the characteristic potential for activation of anodic dissolution due to Pb electro-desorption. Figure 1b shows the relation between logarithm of anodic current density, i_a, and electrode potential, E, obtained from the anodic polarization curves of Fig. 1a. The anodic Tafel slopes, b^+, obtained from the linear relation between log i_a and E are b^+ = 34 mV $decade^{-1}$ in the absence of Pb^{2+} and b^+ = 8.5 mV $decade^{-1}$ in the presence of 10^{-3} M Pb^{2+}. It has been reported that the anodic Tafel slope, b^+, of pure Fe in acidic perchlorate solution (pH 1~2) changes from 63 ± 5 mV $decade^{-1}$ in non-stationary state to 30 ± 4 mV $decade^{-1}$ in stationary state [19]. The value of b^+ = 34 mV $decade^{-1}$ in the present study is close to that in stationary state. The value of b^+ = 8.5 mV $decade^{-1}$ in the presence of 10^{-3} M Pb^{2+} is significantly small as compared with that of 34 mV $decade^{-1}$ in the absence of Pb^{2+}. Similar results were previously reported for the effect of Pb^{2+} on anodic dissolution of pure Ni [8]. The low Tafel slope of pure Fe in the presence of Pb^{2+} is explained in terms of the increase in bare surface sites available for anodic dissolution due to Pb electro-desorption.

To confirm whether Pb-bulk deposition does influence the anodic dissolution of Fe, the Fe specimen was polarized in solution with 10^{-3} M Pb^{2+} at a potential sweep rate of 1.0 mV s^{-1} from E_{ocp} to $E_{c,l}$ and then from $E_{c,l}$ to $E_{a,l}$. The value of $E_{c,l}$ was set to - 0.275 V (SHE), which is less noble by 60 mV than E_{eq} (10^{-3} M Pb^{2+} / Pb) = - 0.215 V (SHE). Figure 2a shows the polarization curve (solid line) of pure Fe obtained with the above procedure. A small anodic current peak appears at around - 0.2 V (SHE) during anodic potential sweep from $E_{c,l}$ to $E_{a,l}$. The part of the anodic polarization curve in the potential range between $E_{c,l}$ and E = - 0.165 V (SHE) extracted from Fig. 2a is magnified in Fig. 2b to quantify the

small anodic current peak. The anodic peak area surrounded by the polarization curve and dotted lines drawn in Fig. 2b would correspond to the electric charge, Q_a, required for anodic striping of the bulk-deposited Pb. Q_a obtained from the anodic peak is 7.86 mC cm^{-2}. The electric charge, $Q_{Pb\text{-}mono}$ required for the formation of Pb-monolayer on polycrystalline Fe can be roughly calculated by using the following equations.

$$Q_{Pb-mono} = \frac{2F\Gamma_{Pb-mono}}{N_A} \qquad (1)$$

where F is the Faraday constant, $\Gamma_{Pb\text{-}mono}$, the surface atomic density corresponding to Pb-monolayer on pure Fe and N_A is the Avogadro number. In Eq. (1), it is assumed that the complete discharge reaction of Pb^{2+} to metallic Pb occurs on Fe surface. Furthermore, the value of $\Gamma_{Pb\text{-}mono}$ can be estimated by using Eq. (2), assuming that the ratio of area occupied by adsorbate and substrate atoms is proportional to square of the ratio of effective atomic radii.

$$\Gamma_{Pb-mono} = \phi_{Fe}\Gamma_{Fe}\left(\frac{r_{Fe}}{r_{Pb}}\right)^2 \qquad (2)$$

where ϕ_{Fe} is the roughness factor of the Fe surface, Γ_{Fe}, the surface atomic density of Fe for the uppermost Fe surface, and r_{Fe} and r_{Pb} are the effective radii of Fe and Pb, respectively. Using Γ_{Fe} = 1.21 x 10^{15} atoms cm^{-2} (assuming equivalent distribution of (110), (100) and (111) planes), r_{Fe} = 1.26 Å, r_{Pb} = 1.39 Å and ϕ_{Fe} = 1.3 (for the Fe surface polished with 0.3 μm-alumina abrasives) [20, 21], $\Gamma_{Pb\text{-}mono}$ = 1.3 x 10^{15} atoms cm^{-2} is obtained from Eq. (2). It should be remarked that r_{Pb} = 1.39 Å is determined from the Pb-Ni bond distance obtained for Pb-UPD on Ni [15] and is different from r_{Pb} = 1.75 Å of bulk crystalline Pb. $Q_{Pb\text{-}mono}$ = 420 μC cm^{-2} for pure Fe is eventually obtained from Eq. (1). Q_a = 7.86 mC cm^{-2} in Fig. 2b is about 20 times as much as $Q_{Pb\text{-}mono}$ = 420 μC cm^{-2}, proving that the anodic peak is originated from the anodic stripping of bulk-deposited Pb.

As shown in Fig. 2b, the cathodic current peak corresponding to Pb-bulk deposition during cathodic potential sweep from E_{ocp} to $E_{c,l}$ is broad and not clear because of overlapping with hydrogen-evolution current. For comparison, the polarization curve (dotted line) obtained by direct-anodic potential sweep from E_{ocp} to $E_{a,l}$ is also shown in Fig. 2a. Both polarization curves coincide each other at the potentials more noble than E_{ocp} indicating that there is no significant hysteresis for polarization behavior at a potential sweep rate of 1.0 mV s^{-1} and thus, the influence of Pb-bulk deposition on anodic dissolution of Fe is negligibly small.

Polarization behavior of Fe-30 Ni alloy

Figure 3a shows the anodic polarization curves of Fe-30 Ni alloy obtained with a potential sweep (1.0 mV s^{-1}) from E_{ocp} to $E_{a,l}$ in deaerated 0.1 M $NaClO_4$ + 10^{-2} M $HClO_4$ solutions without and with 10^{-3} M Pb^{2+}. The value of $E_{a,l}$ was set to 0.240 V (SHE). The steady state values of E_{ocp} in solutions without and with 10^{-3} M Pb^{2+} are - 0.145 ± 0.003 V and - 0.097 ± 0.036 V (SHE), respectively. The value of E_{ocp} in solution with 10^{-3} M Pb^{2+}fluctuates largely as compared with that in solution without 10^{-3} M Pb^{2+}. Nevertheless, the value of E_{ocp} shifts toward noble direction due to addition of 10^{-3} M Pb^{2+} Fig. 3a

indicates that Pb^{2+} inhibits the anodic dissolution of Fe-30 Ni alloy and promotes the passivation. The Pb species adsorbed on Fe-30 Ni alloy as well as on pure Fe would block the active dissolution sites, which would induce the inhibition of anodic dissolution. The large fluctuation in E_{ocp} in solution with 10^{-3} M Pb^{2+}may result from the heterogeneity in surface structure or surface composition of the Fe-30 Ni alloy specimens although the cause is not clear. The anodic polarization curves of two Fe-30 Ni alloy specimens A and B with different induction periods (τ_A = 15 mV and τ_B = 88 mV) as an extreme case are shown in Fig. 3b, indicating that the potential of rapid increase in anodic dissolution current, $E_{i,a}$ = - 0.043 ± 0.008 V does not sensitively depend on the specimens in spite of the large fluctuation in E_{ocp}. For the specimen B with τ_B = 88 mV, small anodic current flows during induction period and increases up to about 10 μA cm^{-2} at $E_{i,a}$. This small anodic current may be ascribed to anodic dissolution of Fe from the small surface fraction enriched with Fe component which would not be covered with Pb. In contrast, the main surface fraction with the alloy composition is covered with Pb and the anodic dissolution of Fe-30 Ni alloy is enhanced at $E_{i,a}$ when the Pb electro-desorption proceeds from the main surface fraction.

Figure 3c shows the relation between logarithm of anodic current density, i_a, and electrode potential, E, obtained from the anodic polarization curves of Fig. 3a. The anodic Tafel slopes, b^+, obtained from the linear relation between log i_a and E are b^+ = 39 mV $decade^{-1}$ in the absence of Pb^{2+} and b^+ = 9.0 mV $decade^{-1}$ in the presence of 10^{-3} M Pb^{2+}. It has been reported that the anodic Tafel slope, b^+, of pure Ni in acidic perchlorate solution changes from 66 ± 7 mV $decade^{-1}$ in non-stationary state to 37 ± 4 mV $decade^{-1}$ in stationary state [22, 23]. b^+ = 39 mV $decade^{-1}$ in the absence of Pb^{2+} is close to that in stationary state, while b^+ = 9.0 mV $decade^{-1}$ in the presence of 10^{-3} M Pb^{2+} is significantly low. The low Tafel slope in the presence of $Pb^{2+}$for Fe-30 Ni alloy is also explained in terms of the increase of active dissolution sites due to Pb electro-desorption.

Figure 4 shows the polarization curve of the Fe-30 Ni alloy obtained with a potential sweep (1.0 mV s^{-1}) from E_{ocp} to $E_{c,l}$ = - 0.275 V (SHE) and then from $E_{c,l}$ to anodic direction in solution with 10^{-3} M Pb^{2+}. In the cathodic potential sweep, the cathodic current peak appears at - 0.248 V (SHE), while in the anodic potential sweep, the anodic current peak appears at - 0.211 V (SHE). The potential of anodic current peak is close to E_{eq} (10^{-3} M Pb^{2+} / Pb) = - 0.215 V (SHE). The electric charge of the anodic current peak in Fig. 4 is Q_a = 4.15 mC cm^{-2}. The surface atomic density, $\Gamma_{Pb\text{-}mono}$, corresponding to Pb-monolayer on pure Ni can be estimated by using Eq. (3).

$$\Gamma_{Pb-mono} = \phi_{Ni}\Gamma_{Ni}\left(\frac{r_{Ni}}{r_{Pb}}\right)^2 \qquad (3)$$

where ϕ_{Ni} is the roughness factor of the Ni surface, Γ_{Ni}, the surface atomic density of Ni for the uppermost Ni surface, and r_{Ni} and r_{Pb} are the effective radii of Ni and Pb, respectively. Using Γ_{Ni} = 1.82 x 10^{15} atoms cm^{-2} (assuming equivalent distribution of (111), (100) and (110) planes), r_{Ni} = 1.25 Å, r_{Pb} = 1.39 Å and ϕ_{Ni} = 1.3 (for the Ni surface polished with 0.3 μm-alumina abrasives) [20, 21], $\Gamma_{Pb\text{-}mono}$ = 1.9 x 10^{15} atoms cm^{-2} is obtained from Eq. (3). $Q_{Pb\text{-}mono}$ = 602 μC cm^{-2} for pure Ni is eventually obtained from Eq. (1). Provided that the values of $Q_{Pb\text{-}mono}$ for pure Fe and Ni are allotted in proportion to the alloy composition, $Q_{Pb\text{-}mono}$ = 470 μC cm^{-2} is obtained for Fe-30 Ni alloy. Q_a = 4.15 mC cm^{-2} in Fig. 4 is

about 9 times as much as $Q_{Pb\text{-}mono}$ for Fe-30 Ni alloy, indicating that the anodic current peak at - 0.211 V (SHE) is originated from the anodic stripping of bulk-deposited Pb. The cathodic current peak at - 0.248 V (SHE) in Fig. 4 corresponds to the bulk deposition of Pb. The quantification of the bulk deposition of Pb from the cathodic current peak, however, seems difficult because of overlapping with cathodic current for hydrogen evolution. Besides, no clear cathodic or anodic current peaks associated with Pb electro-adsorption or electro-desorption are observed in the potential region between E_{eq} = - 0.215 V and $E_{i,a}$ = - 0.043 V (SHE).

Polarization behavior of Fe-70 Ni alloy

Figure 5a shows the anodic polarization curves of Fe-70 Ni alloy obtained with a potential sweep (1.0 mV s^{-1}) from E_{ocp} to $E_{a,l}$ in deaerated 0.1 M $NaClO_4$ + 10^{-2} M $HClO_4$ solutions without and with 10^{-3} M Pb^{2+}. The value of $E_{a,l}$ was set to 0.240 V (SHE). The steady state values of E_{ocp} in solutions without and with 10^{-3} M Pb^{2+} are - 0.095 ± 0.002 V and 0.03 ± 0.01 V (SHE), respectively. The addition of 10^{-3} M Pb^{2+} shifts E_{ocp} toward noble direction by 0.125 V and reduces the anodic current peak by 2.3 times, i.e., it promotes passivation. In solution with 10^{-3} M Pb^{2+}, the fluctuation of E_{ocp} for Fe-70 Ni alloy is significantly small as compared with that for Fe-30 Ni alloy, which reflects on good reproducible values of τ = 8 ± 4 mV and $E_{i,a}$ = 0.040 ± 0.002 V. The above good reproducible results may result from the uniformity in surface structure or surface composition of the Fe-70 Ni alloy specimen. The inhibition or enhancement of anodic dissolution for Fe-70 Ni alloy are explained in terms of Pb electro-adsorption or electro-desorption, respectively as described above for pure Fe and Fe-30 Ni alloy. Figure 5b shows the relation between logarithm of anodic current density, i_a, and electrode potential, E, obtained from the anodic polarization curves of Fig. 5a. The anodic Tafel slopes, b^+, obtained from the linear relation between log i_a and E are b^+ = 40 mV $decade^{-1}$ in the absence of Pb^{2+} and b^+ = 15 mV $decade^{-1}$ in the presence of 10^{-3} M Pb^{2+}. The low Tafel slope in the presence of Pb^{2+} for Fe-70 Ni alloy as well as Fe- 30 Ni alloy is also explained in terms of the increase of bare surface sites available for anodic dissolution due to Pb electro-desorption.

Figure 6 shows the polarization curve of the Fe-70 Ni alloy obtained with a potential sweep (1.0 mV s^{-1}) from E_{ocp} to $E_{c,l}$ = - 0.275 V (SHE) and then from $E_{c,l}$ to anodic direction in solution with 10^{-3} M Pb^{2+}. In the cathodic potential sweep, the cathodic current peak appears at - 0.247 V (SHE), while in the anodic potential sweep, the anodic current peak appears at - 0.208 V (SHE). The potential of anodic current peak is close to the equilibrium potential of 10^{-3} M Pb^{2+}/ Pb. The electric charge of the anodic current peak in Fig. 6 is Q_a = 4.70 mC cm^{-2}. As well as Fe-30 Ni alloy, assuming that the values of $Q_{Pb\text{-}mono}$ for pure Fe and Ni are allotted in proportion to the alloy composition, $Q_{Pb\text{-}mono}$ = 544 μC cm^{-2} is obtained for Fe-70 Ni alloy. Q_a in Fig. 6 is about 9 times as much as $Q_{Pb\text{-}mono}$ for Fe-70 Ni alloy, indicating that the anodic current peak at – 0.208 V (SHE) is originated from the anodic stripping of bulk-deposited Pb.

Figure 7 shows the polarization curve of the Fe-70 Ni alloy obtained with a potential sweep (1.0 mV s^{-1}) from E_{ocp} to $E_{c,l}$ = - 0.215 V (SHE) and then from $E_{c,l}$ to anodic direction in solution with 10^{-3} M Pb^{2+}. The broad current peaks appear in both cathodic and anodic potential sweeps, which may be associated with Pb electro-adsorption and electro-desorption, respectively. The background current

represented by dotted horizontal line drawn in Fig. 7 is - 4.2 μA cm^{-2}. The cathodic current of hydrogen evolution for Fe-70 Ni alloy in solution without 10^{-3} M Pb^{2+} flows at the potential less noble than - 0.10 V (SHE). It is deduced that the cathodic background current in Fig. 7 results from the cathodic reduction of residual oxygen in solution. The electric charges, Q_{I} and Q_{II}, for two areas separated by two dotted lines in Fig. 7 may be assigned to the cathodic charge for electro-adsorption of Pb and the anodic charge for electro-desorption of Pb, respectively. As a result, $Q_{\mathrm{I}} \approx Q_{\mathrm{II}} \approx 250$ μC cm^{-2} is obtained, which is about half times as much as $Q_{\mathrm{Pb\text{-}mono}} = 544$ μC cm^{-2} for Fe-70 Ni alloy, i.e., corresponding to the surface coverage of Pb, $\theta_{\mathrm{Pb}} \approx 0.46$. Assuming $\theta_{\mathrm{Pb}} \approx 1.0$ at – 0.215 V (SHE) [8], this means that the surface coverage of Pb at E_{ocp} is $\theta_{\mathrm{Pb}} \approx 0.54$.

Potential window of Pb-UPD associated with the inhibition of anodic dissolution.

The average values of E_{ocp}, $E_{\mathrm{i,a}}$ and b^{+} obtained for pure Fe, Fe-30 Ni alloy and Fe-70 Ni alloy in 0.1 M $NaClO_4$ + 10^{-2} M $HClO_4$ solutions without and with 10^{-3} M Pb^{2+} are listed in Table 2. For comparison, the average values of E_{ocp}, $E_{\mathrm{i,a}}$ and b^{+} obtained previously under the same experimental conditions for pure Ni [8] are also listed in Table 2. There were no induction periods, i.e., $E_{\mathrm{ocp}} = E_{\mathrm{i,a}}$ for pure Ni in the presence of Pb^{2+}[8]. In this section, discussion is focused on the potential window of Pb-UPD associated with the inhibition of anodic dissolution. Kolb et al. [9,10] found the following empirical relation between the potential window of UPD, ΔE_{UPD} and the difference in work-function between substrate metal, M', and adsorbed metal, M.

$$\Delta E_{UPD} \approx 0.5 \frac{(\Phi_{M'} - \Phi_{M})}{e} \quad (4)$$

where $\Phi_{\mathrm{M'}}$ and Φ_{M} are the work-functions of substrate metal, M', and of adsorbed metal, M, respectively and e is the elementary charge. The relation represented by Eq. (4) holds on many UPD systems in which noble metals such as Pt, Au and Ag are used as substrate metals [9.10]. Since noble metals are not susceptible to corrosion or anodic dissolution, the cathodic and anodic current peaks corresponding to electro-adsorption and electro-desorption of UPD species can be easily observed in the polarization curves of the substrate noble metals. Kolb et al. [9,10] determined experimentally ΔE_{UPD} as the difference between two characteristic potentials, $E_{\mathrm{M,b}}$ and $E_{\mathrm{M,s}}$, from the polarization curve of the substrate noble metal, M', measured in solution containing M^{z+} by anodic potential sweep from a potential less noble than the equilibrium potential of M^{z+} /M.

$$\Delta E_{UPD} = E_{M,s} - E_{M,b} \quad (5)$$

where $E_{\mathrm{M,b}}$ and $E_{\mathrm{M,s}}$ are the potentials at anodic current peaks corresponding to anodic stripping of bulk-deposited species and to electro-desorption of UPD species, respectively. In the cases of base metals such as pure Fe and Fe-Ni alloys that are susceptible to corrosion or anodic dissolution, however, the experimental determination of ΔE_{UPD} is difficult since no clear current peak corresponding to electro-desorption of UPD species appears due to overlapping with anodic dissolution current of substrate metal. Nevertheless, ΔE_{UPD} may be evaluated from Eq. (4). The work-functions, $\Phi_{\mathrm{Fe\text{-}Ni}}$, of Fe-Ni alloys are unknown but can be estimated by allotting the work-functions, Φ_{Fe} and Φ_{Ni}, of pure Fe and Ni in proportion to the alloy composition.

$$\Phi_{Fe-Ni} = (1 - X_{Ni})\Phi_{Fe} + X_{Ni}\Phi_{Ni} \quad (6)$$

where X_{Ni} is the atomic fraction of Ni component in Fe-Ni alloy. The values of $\Phi_{\text{Fe-30 Ni}}$ (X_{Ni} = 0.284) and $\Phi_{\text{Fe-70 Ni}}$ (X_{Ni} = 0.683) calculated by using Eq. (6) in addition to the values of Φ_{Fe} and Φ_{Ni} are listed in Table 3. Furthermore, the differences in work-functions between substrate metals and adsorbed Pb, $\Phi_{M'} - \Phi_{Pb}$, are listed in Table 3. The potential window of Pb-UPD, $\Delta E_{\text{Pb-UPD}}$, can be estimated from the value of $\Phi_{M'} - \Phi_{Pb}$ in Table 3. The inhibition of anodic dissolution by Pb-UPD would continue as far as θ_{Pb} exceeds a critical value, $\theta_{Pb,c}$. When θ_{Pb} is reduced to $\theta_{Pb,c}$ due to electro-desorption of Pb, the inhibition of anodic dissolution would cease to induce the rapid increase in anodic current at $E_{i,a}$. The value of $\theta_{Pb,c} \approx 0.37$ was estimated for pure Ni [8]. The polarization curve in Fig. 7 provides the estimated value of $\theta_{Pb,c} \approx 0.5 \sim 0.6$ at $E_{i,a}$ = 0.04 V (SHE) for Fe-70 Ni alloy. The coulometric estimation of $\theta_{Pb,c}$ for pure Fe and Fe-30 Ni alloy is difficult because there is no clear cathodic or anodic current peak associated with electro-adsorption or electro-desorption of Pb in polarization curve. Besides, $E_{i,a}$ for pure Fe is close to E_{eq} (10^{-3} M Pb^{2+} / Pb) = - 0.215 V (SHE). If taken into consideration that pure Fe and Fe-30 Ni alloy are more susceptible to corrosion than Fe-70 Ni alloy and pure Ni, a higher value of $\theta_{Pb,c}$ may be requisite at $E_{i,a}$ for pure Fe and Fe- 30 Ni alloy. Kolb et al. [10] estimated coulometrically $\theta_M \approx 0.2$ at $E_{M,s}$ with respect to various UPD species on noble metals. There is an indication that the values of $\theta_{Pb,c}$ in the present work are higher than the values of θ_M [10]. Since anodic dissolution of pure Fe and Fe-Ni alloys is competitive with Pb electro-adsorption, a high surface coverage of Pb would be required for the inhibition of anodic dissolution as compared with the case in which no anodic dissolution takes place. This suggests that $E_{i,a}$ corresponding to $\theta_{Pb,c}$ is less noble than $E_{M,s}$.

The values of $E_{i,a}$ in Table 2 are referred to E_{eq} (10^{-3} M Pb^{2+} / Pb) = - 0.215 V (SHE) for comparison with ΔE_{UPD}. In Fig. 8, $\Delta E_{i,a} = E_{i,a} - E_{eq}$ (10^{-3} M Pb^{2+} / Pb) is plotted versus $\Delta E_{\text{Pb-UPD}}$. The values of $\Delta E_{\text{Pb-UPD}}$ in the abscissa of Fig. 8 were obtained by substituting the values of $\Phi_{M'} - \Phi_{Pb}$ in Table 3 into Eq. (4). The dotted linear line with a slope of unity in Fig. 8 is plotted for checking the equality between $\Delta E_{i,a}$ and $\Delta E_{\text{Pb-UPD}}$. The ordinate level of the solid curve representing the relation between $\Delta E_{i,a}$ and $\Delta E_{\text{Pb-UPD}}$ is lower than that of the dotted line, indicating that $\Delta E_{i,a}$ is located within $\Delta E_{\text{Pb-UPD}}$, which confirms that the inhibition of anodic dissolution is caused by Pb-UPD. The relation between $\Delta E_{i,a}$ and $\Delta E_{\text{Pb-UPD}}$ deviates upward from the linearity which may be originated from the estimation of work-functions of Fe-Ni alloys by Eq. (6). The surface composition of alloy is not always same as the bulk composition. The work-function of binary alloy is sensitive to the surface composition [24]. The upward deviation of the relation between $\Delta E_{i,a}$ and $\Delta E_{\text{Pb-UPD}}$ from the linearity suggests that the alloy surface is enriched with Ni component as compared with bulk composition. The surface enrichment of Ni component increases the work-function of Fe-Ni alloy by which the data points of Fe-Ni alloys shift toward right side in Fig. 8. If the increase in work-function of Fe-Ni alloy due to surface enrichment of Ni component is taken into consideration, the relation between $\Delta E_{i,a}$ and $\Delta E_{\text{Pb-UPD}}$ would approach to the linearity.

It has been reported that the oxide film on Fe-Ni alloy formed in air at room temperature or in oxygen at 433 ~ 473 K is enriched with Fe component while the metallic side near the oxide film / alloy

interface is enriched with Ni component [25, 26]. The Fe-enriched oxide film would dissolve easily in acidic perchlorate solution (pH 1.9) used in this study to provide the Ni-enriched alloy surface without oxide film. Although no in-situ analyses of surface composition of Fe-Ni alloy have been made in the present work, the relation between $\Delta E_{i,a}$ and $\Delta E_{Pb\text{-}UPD}$ should approach to the linearity if the surface composition in place of the bulk composition were employed in Eq. (6). It has been reported that the relation between work-function and bulk alloy composition deviates from the linearity for the Ag-Au binary alloys known as a full solubility binary system [24, 27]. The deviation from the linearity was explained in terms of the surface alloy composition being enriched with Ag component. Moreover, it has been confirmed that the work-function changes linearly with bulk alloy composition in the case where Cu-Ni binary alloys with a miscibility have no surface enrichment of Cu component due to sputtering of the surface layers [24, 28]. The above results also supports that the upward deviation of the relation between $\Delta E_{i,a}$ and $\Delta E_{Pb\text{-}UPD}$ from the linearity results from the surface enrichment of Ni component.

Conclusions

The potentiodynamic polarization curves of pure Fe, Fe-30 Ni and Fe-70 Ni alloys in acidic perchlorate solutions (pH 1.9) without and with 10^{-3} M Pb^{2+} were recorded to investigate the effect of Pb-UPD on anodic dissolution and passivation in relation to Pb-SCC of Ni base alloys. The following conclusions were drawn:

1. The addition of 10^{-3} M Pb^{2+} shifts the open-circuit potentials, E_{ocp}, of pure Fe and Fe-Ni alloys toward noble direction to inhibit the anodic dissolution and promote the passivation. The inhibition of anodic dissolution was explained in terms of the active dissolution sites being blocked with electro-adsorbed Pb on substrate metal.
2. The anodic dissolution of pure Fe and Fe-Ni alloys in the presence of 10^{-3} M Pb^{2+} is enhanced as the Pb electro-desorption proceeds with anodic potential sweep. The anodic dissolution increases rapidly when the surface coverage of Pb, θ_{Pb}, is reduced to a critical level, $\theta_{Pb,c}$ at $E_{i,a}$.
3. Tafel slopes (b^+ = 8.5 ~ 15 mV decade^{-1}) of anodic dissolution for pure Fe and Fe-Ni alloys in the presence of Pb^{2+} are significantly low as compared with those (b^+ = 34 ~ 40 mV decade^{-1}) in the absence of Pb^{2+}, which reflects on the rapid increase of active dissolution sites as a result of Pb electro-desorption.
4. The potential windows of Pb-UPD, $\Delta E_{Pb\text{-}UPD}$, were estimated from the differences in work-function between substrate metals and Pb. The potentials, $E_{i,a}$, were referred to the equilibrium potential (10^{-3} M Pb^{2+}/ Pb), E_{eq} = - 0.215 V (SHE) for comparison with $\Delta E_{Pb\text{-}UPD}$. The values of $\Delta E_{i,a} = E_{i,a} - E_{eq}$ are located within $\Delta E_{Pb\text{-}UPD}$ confirming that the inhibition of anodic dissolution is caused by Pb-UPD.

References

1. Staehle RW (2004) Proc. 11 th International Conference on Environmental Degradation of Materials in Nuclear Power Systems-Water Reactors. American Nuclear Society, p 381-424.
2. Staehle RW (2005) Proc. 12 th International Conference on Environmental Degradation of Materials in Nuclear Power Systems-Water Reactors, Minerals, Metals and Materials Society, p 163-1210.
3. Lu YC (2005) Proc. 12 th International Conference on Environmental Degradation of Materials in Nuclear Power Systems-Water Reactors. Minerals, Metals and Materials Society, p 1211-1219.
4. Lu BT, Luo JL, Yu YC (2007) J Electrochem Soc 154: C379-C389.
5. Costa D, Talah H, Marcus P, le Cavar M, Gelpi A (1995) Proc. 7 th International Conference on Environmental Degradation of Materials in Nuclear Power Systems-Water Reactors. NACE, Houston, p 199-208.
6. Hwang SS, Kim JS (2002) Corrosion 58: 392-398.
7. Radhakrishnan H, Carcea AG, Newman RC (2005) Corros Sci 47: 3234-3248.
8. Seo M, Fushimi K, Habazaki H, Nakayama T (2008) Corros Sci 50: 3139-3146.
9. Kolb DM, Prazasnyski M, Gerischer H (1974) J Electroanal Chem 54: 25-38.
10. Kolb DM (1978) In Gerischer H, Tobias CW (eds) Advances in Electrochemistry and Electrochemical Engineering vol 11. Physical and Electrochemical Properties of Metal Monolayers on Metallic Substrates. John Wiley & Sons, New York, p 125-271.
11. Herrero E, Buller LJ, Abruna HD (2001) Chem Rev 101: 1897-1930.
12. Lafranconi G, Mazza F, Sivieri E, Torchio S. (1978) Corros Sci 18: 617-629.
13. Drazic DM, Vorkapic LZ (1978) Corros Sci 18: 907-910.
14. Jüttner K (1980) Werkstoffe und Korrosion 31: 358-363.
15. Seo M, Fushimi K, Aoki Y, Habazaki H, Inaba M, Yokomizo M, Hayakawa T, Nakayama T (2012) J Electroanal Chem 671: 7-15.
16. Koma A, Yagi M, Tsukada M, Aono M (1987) Handbook of Surface Physics Technology. Maruzen Co. Tokyo, p 535.
17. Economy G, Speiser R, Beck FH, Fontana MG (1961) J Electrochem Soc 108: 337-343.
18. Condit DO (1972) Corros Sci 12: 451-462.
19. Heusler KE (1982) In Bard AJ (ed) Encyclopedia of Electrochemistry of the Elements vol 9A. Marcel Dekker Inc, New York, p 229-381.
20. Brown IJ, Sotiropoulos S (2001) Electrochim Acta 46: 2711-2720.
21. Seo M, Hyono A, Habazaki H, Nakayama T (2014) J Electrochem Soc 161: C550-C556.
22. Heusler KE, Gaiser L (1968) Electrochim Acta 13: 59-60.
23. Arvia AJ, Posadas D (1975) In Bard AJ (ed) Encyclopedia of Electrochemistry of the Elements vol 3. Marcel Dekker Inc, New York, p 298-309.
24. Rothschild JA, Eizenberg M (2010) Phys Rev B 81:224021-1-8.
25. Seo M, Sato N (1978) Corros Sci 18: 577-589.
26. Seo M, Sato N (1983) Oxid Met 19: 151-163.
27. Fain Jr SC, McDavid JM (1974) Phys Rev B 9: 5099-5107.
28. Ishi R, Matsumura K, Sakai A, Sakata T (2001) App Surf Sci 167-170: 658-661.

Figure Captions

Figure 1a Anodic polarization curves of pure Fe obtained with a potential sweep (1.0 mV s^{-1}) from E_{ocp} to $E_{a,l}$ in deaerated 0.1 M $NaClO_4$ + 10^{-2} M $HClO_4$ solutions without and with 10^{-3} M Pb^{2+}. $E_{a,l}$ was set to a potential corresponding to an anodic current density of 8 mA cm^{-2}.

Figure 1b Relation between logarithm of anodic current density, i_a, and electrode potential, E, obtained from the anodic polarization curves of Fig. 1a.

Figure 2a Polarization curve (solid line) of pure Fe obtained with a potential sweep (1.0 mV s^{-1}) from E_{ocp} to $E_{c,l}$ and then from $E_{c,l}$ to $E_{a,l}$ in solution with 10^{-3} M Pb^{2+}. $E_{c,l}$ was set to - 0.275 V (SHE). For comparison, the anodic polarization curve of pure Fe in solution with 10^{-3} M Pb^{2+} in Fig. 1a was represented by the dotted line in Fig. 2a.

Figure 2b Magnified part of the anodic polarization curve in the potential range between $E_{c,l}$ and E = - 0.165 V (SHE) extracted from Fig. 2a.

Figure 3a Anodic polarization curves of Fe-30 Ni alloy obtained with a potential sweep (1.0 mV s^{-1}) from E_{ocp} to $E_{a,l}$ in deaerated 0.1 M $NaClO_4$ + 10^{-2} M $HClO_4$ solutions without and with 10^{-3} M Pb^{2+}. $E_{a,l}$ was set to 0.240 V (SHE).

Figure 3b Anodic polarization curves of two Fe-30 Ni alloy specimens A and B with different induction periods (τ_A = 15 mV and τ_B = 88 mV) as an extreme case in solution with 10^{-3} M Pb^{2+}.

Figure 3c Relation between logarithm of anodic current density, i_a, and electrode potential, E, obtained from the anodic polarization curves of Fig. 3a.

Figure 4 Polarization curve of the Fe-30 Ni alloy obtained with a potential sweep (1.0 mV s^{-1}) from E_{ocp} to $E_{c,l}$ = - 0.275 V (SHE) and then from $E_{c,l}$ to anodic direction in solution with 10^{-3} M Pb^{2+}.

Figure 5a Anodic polarization curves of Fe-70 Ni alloy obtained with a potential sweep (1.0 mV s^{-1}) from E_{ocp} to $E_{a,l}$ in deaerated 0.1 M $NaClO_4$ + 10^{-2} M $HClO_4$ solutions without and with 10^{-3} M Pb^{2+}. $E_{a,l}$ was set to 0.240 V (SHE).

Figure 5b Relation between logarithm of anodic current density, i_a, and electrode potential, E, obtained from the anodic polarization curves of Fig. 5a.

Figure 6 Polarization curve of Fe-70 Ni alloy obtained with a potential sweep (1.0 mV s^{-1}) from E_{ocp} to $E_{c,l}$ = - 0.275 V (SHE) and then from $E_{c,l}$ to anodic direction in solution with 10^{-3} M Pb^{2+}.

Figure 7 Polarization curve of Fe-70 Ni alloy obtained with a potential sweep (1.0 mV s^{-1}) from E_{ocp} to $E_{c,l}$ = - 0.215 V (SHE) and then from $E_{c,l}$ to anodic direction in solution with 10^{-3} M Pb^{2+}. ($Q_I \approx Q_{II} \approx$ 250 μC cm^{-2})

Figure 8 Relation between $\Delta E_{i,a} = E_{i,a} - E_{eq}$ (10^{-3} M Pb^{2+} / Pb) and $\Delta E_{Pb\text{-}UPD}$ for pure Fe, Fe-Ni alloys and pure Ni. The dotted linear line of slope unity is plotted for checking the equality between $\Delta E_{i,a}$ and $\Delta E_{Pb\text{-}UPD}$.

Table 1 Chemical compositions of the specimens (mass%)

	C	Si	Mn	P	S	Cu	Cr	Co	Mo	Ni
Pure Fe	0.0035	0.008	0.0005	0.0024	0.0023	0.002	0.001	—	0.001	0.0040
Fe-30Ni	0.0036	0.005	<0.001	0.003	0.004	<0.01	<0.001	0.020	0.001	29.47
Fe-70Ni	0.0052	0.0118	0.001	0.002	0.001	<0.01	<0.001	0.023	0.001	69.34

Table 2 The average values of E_{ocp}, $E_{i,a}$ and b^+ in 0.1 M $NaClO_4$ + 10^{-2} M $HClO_4$ solutions without and with 10^{-3} M Pb^{2+}.

	without 10^{-3} M Pb^{2+}		with 10^{-3} M Pb^{2+}		
	E_{ocp} / V (SHE)	b^+/mVdecade^{-1}	E_{ocp} / V (SHE)	$E_{i,a}$ / V (SHE)	b^+/mVdecade^{-1}
Pure Fe	- 0.337	34	- 0.206	- 0.185	8.5
Fe-30 Ni	- 0.145	39	- 0.097	- 0.043	9.0
Fe-70 Ni	- 0.095	40	0.030	0.040	15
Pure Ni*	- 0.060	40	0.091	0.091	17

* The data of pure Ni taken from the previous study [8]

Table 3 Work-functions of substrate metals, $\Phi_{M'}$ and the differences in work-function between substrate metals and adsorbed Pb, $\Phi_{M'}-\Phi_{Pb}$.

	$\Phi_{M'}$ / eV	$\Phi_{M'}-\Phi_{Pb}$* / eV
Pure Fe	4.50	0.25
Fe-30 Ni	4.69	0.44
Fe-70 Ni	4.94	0.69
Pure Ni	5.15	0.90

* Φ_{Pb} = 4.25 eV [16]

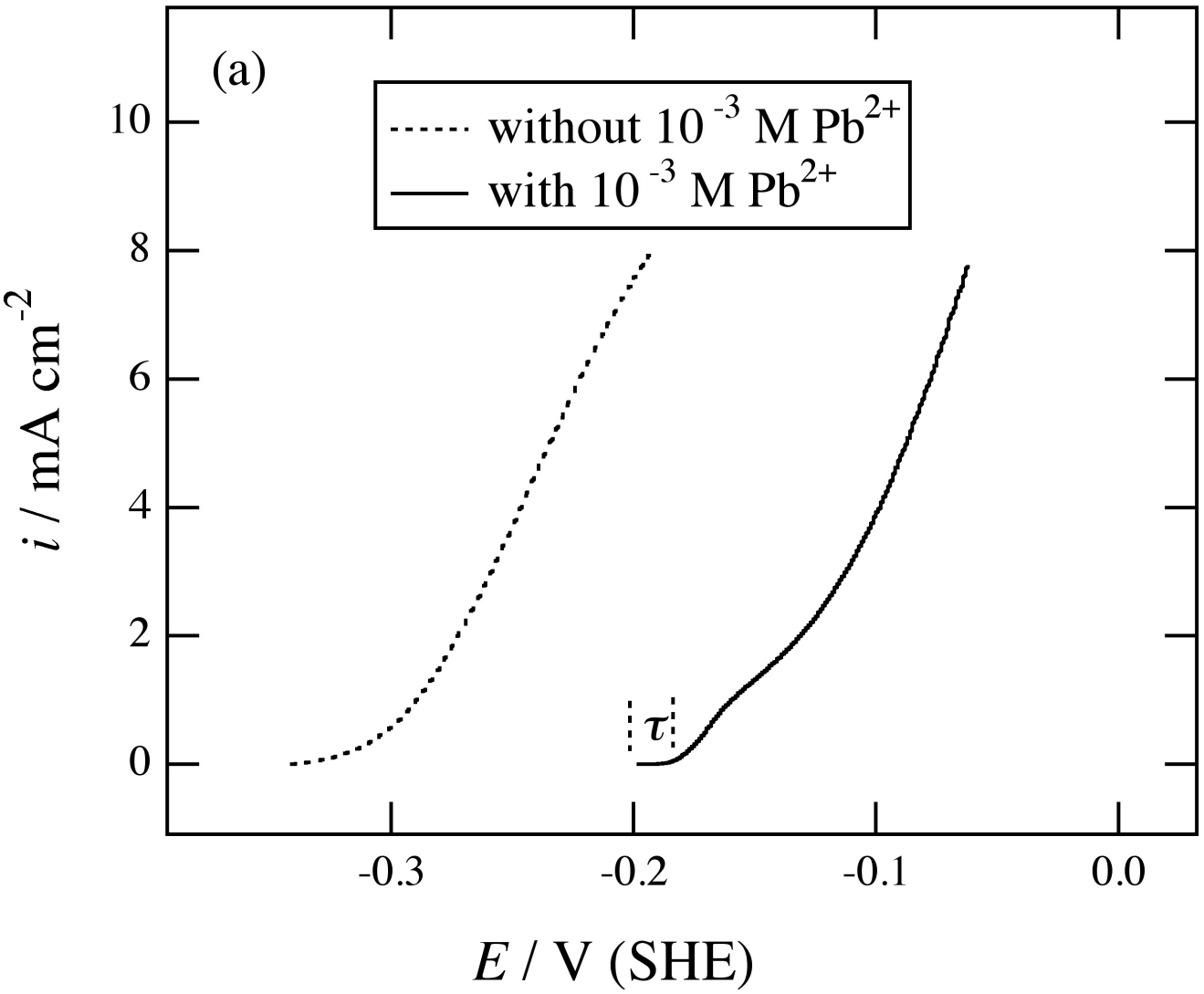
(a)
without 10 -3 M Pb2+
with 10 -3 M Pb2+
τ
i / mA cm-2
E / V (SHE)
10
8
6
4
2
0
-0.3
-0.2
-0.1
0.0

Figure 1a

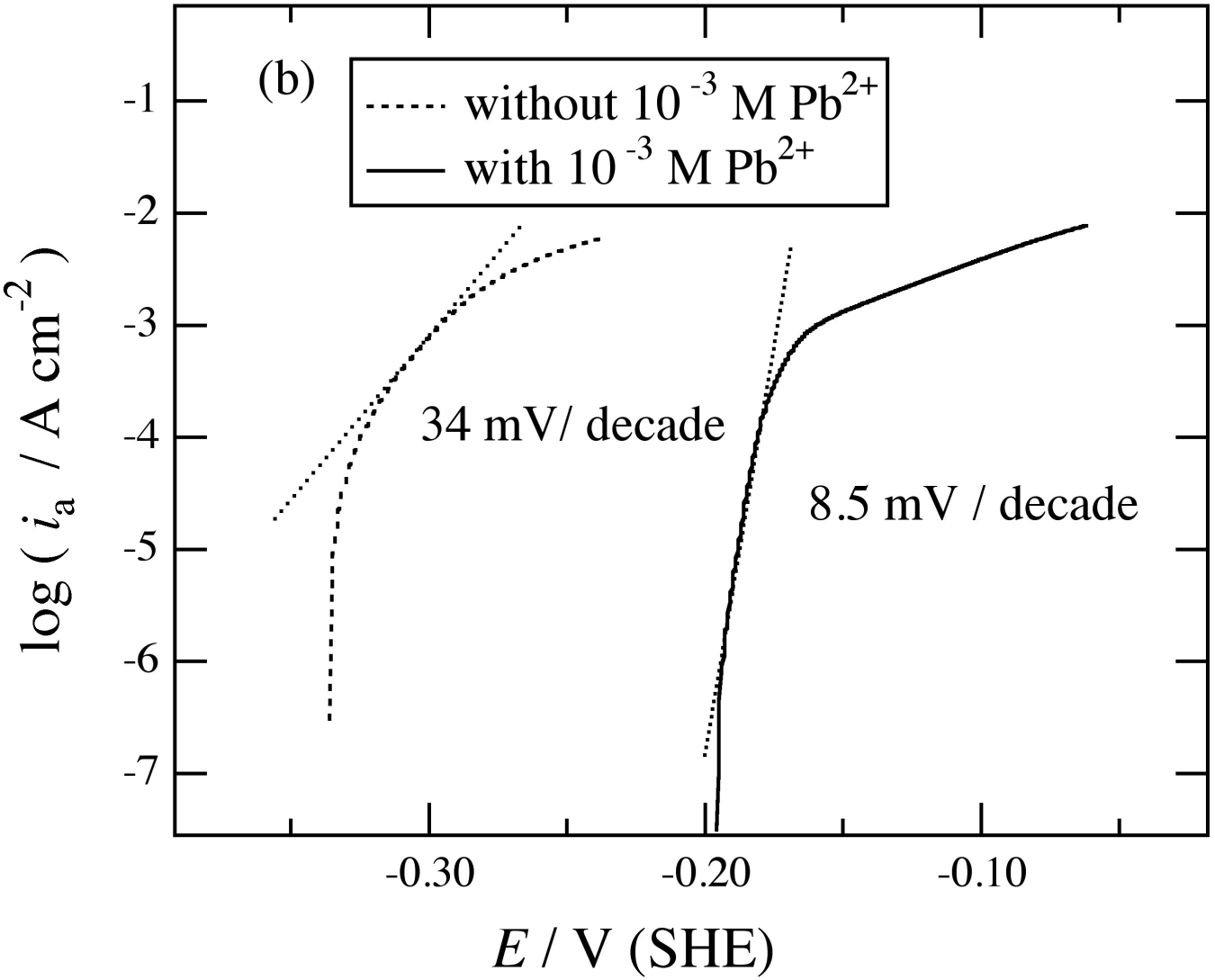
(b)
without 10 -3 M Pb2+
with 10 -3 M Pb2+
34 mV/ decade
8.5 mV / decade
log (ia / A cm-2)
-1
-2
-3
-4
-5
-6
-7
-0.30
-0.20
-0.10
E / V (SHE)

Figure 1b

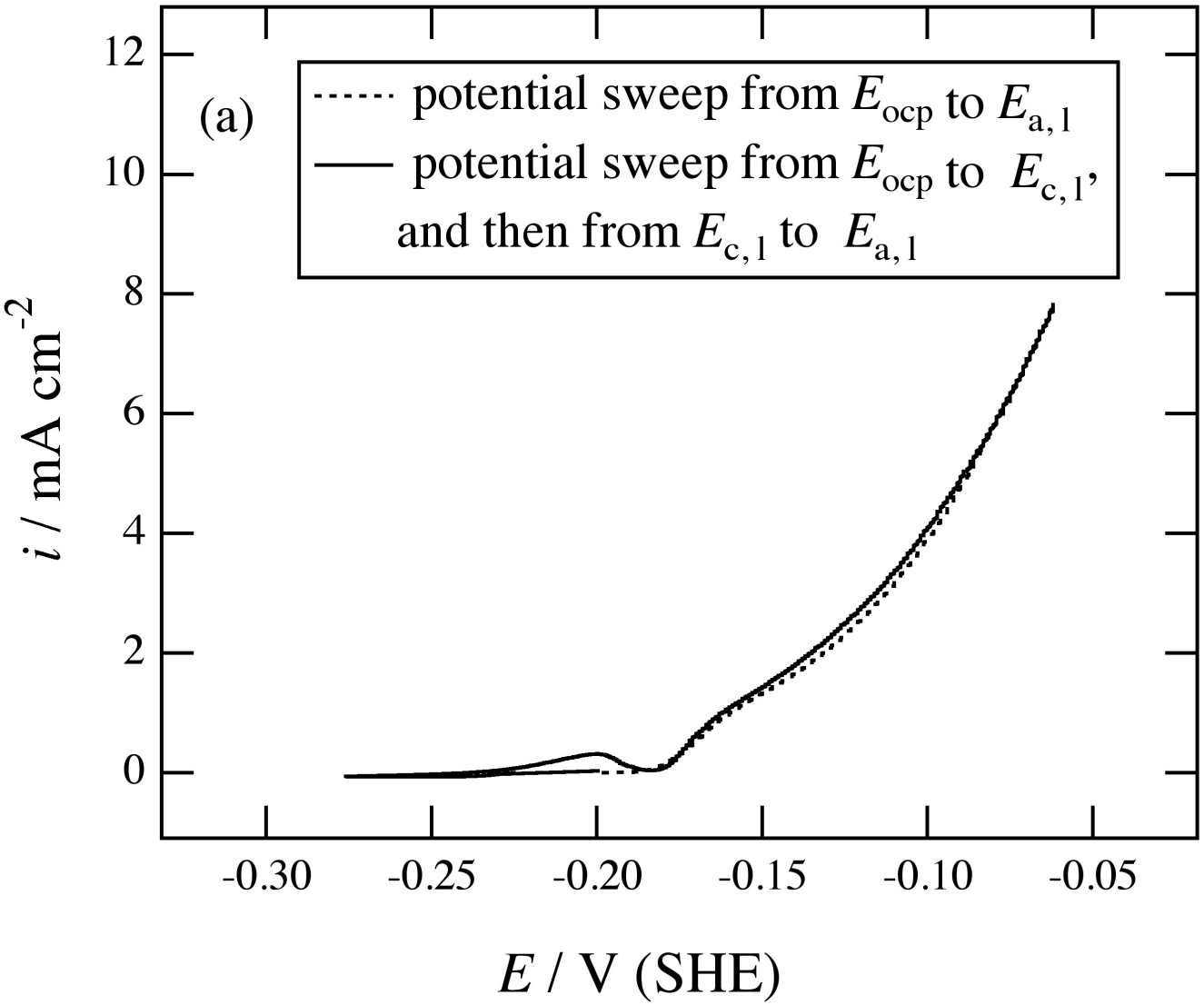
(a)
potential sweep from E_{ocp} to $E_{a,1}$
potential sweep from E_{ocp} to $E_{c,1}$, and then from $E_{c,1}$ to $E_{a,1}$
i / mA cm^{-2}
E / V (SHE)
12
10
8
6
4
2
0
-0.30
-0.25
-0.20
-0.15
-0.10
-0.05

Figure 2a

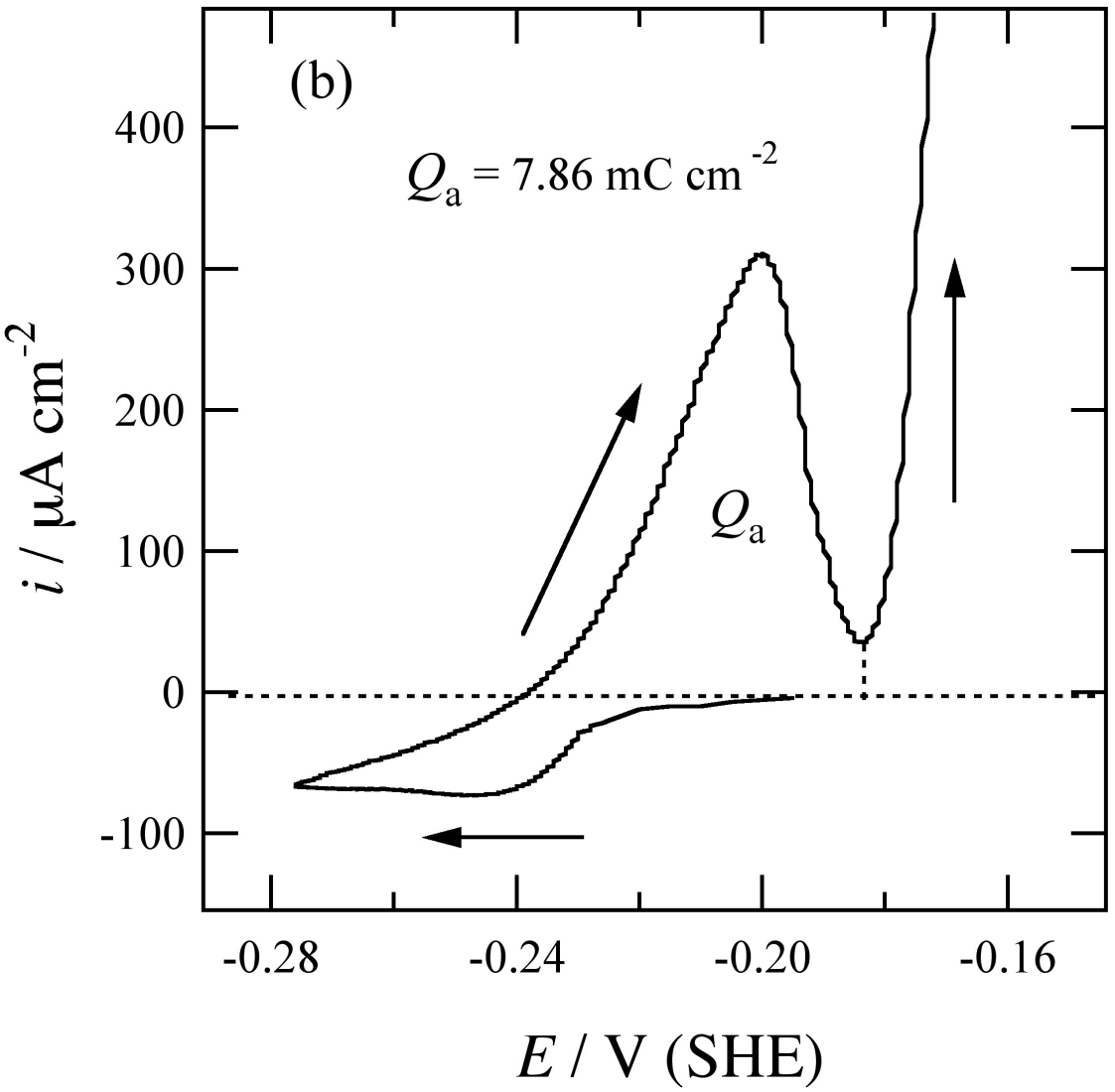
(b)
Q_a = 7.86 mC cm^{-2}
Q_a
400
300
200
100
0
-100
i / μA cm^{-2}
-0.28
-0.24
-0.20
-0.16
E / V (SHE)

Figure 2b

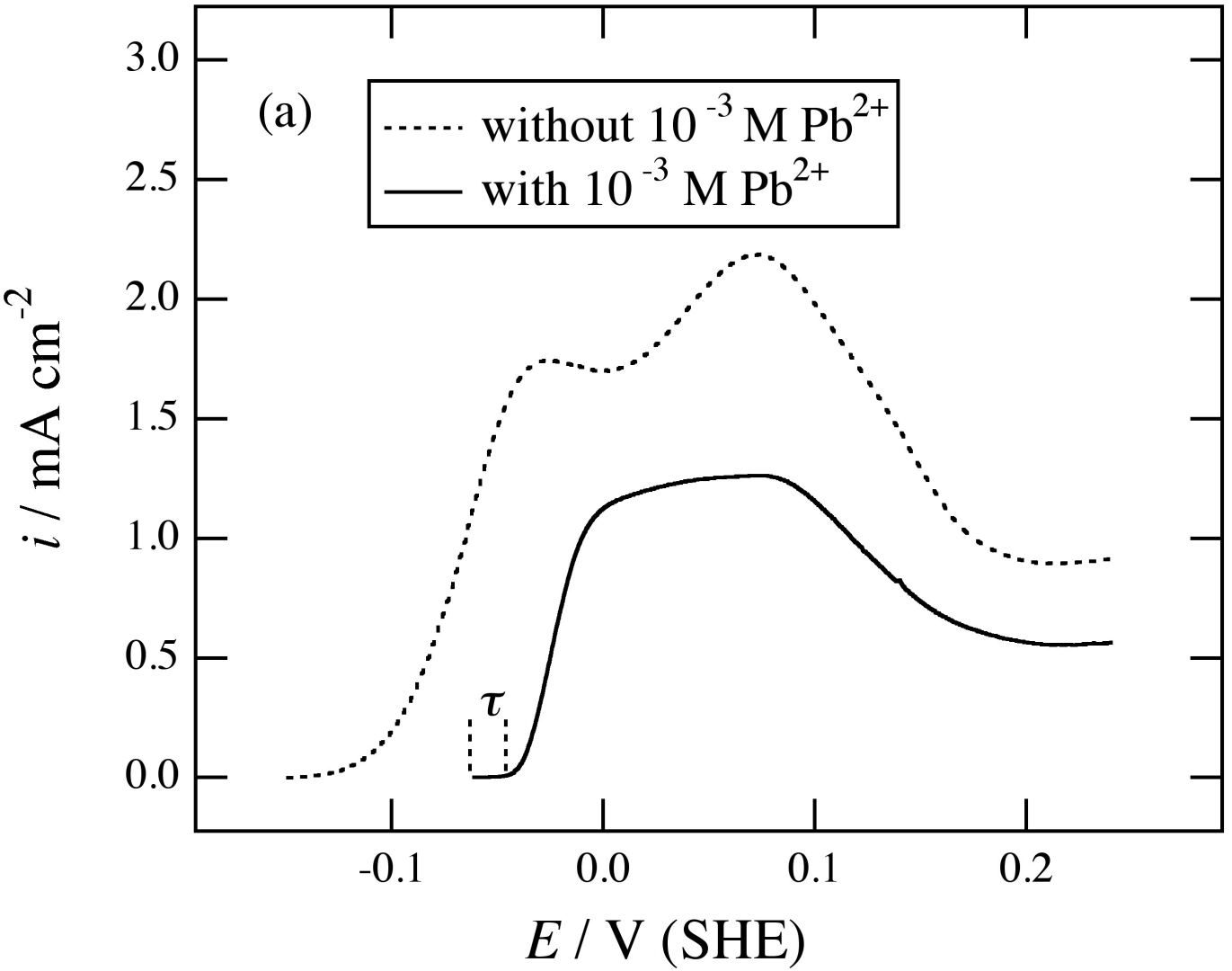
(a)
without 10 -3 M Pb2+
with 10 -3 M Pb2+
τ
i / mA cm-2
E / V (SHE)
3.0
2.5
2.0
1.5
1.0
0.5
0.0
-0.1
0.0
0.1
0.2

Figure 3a

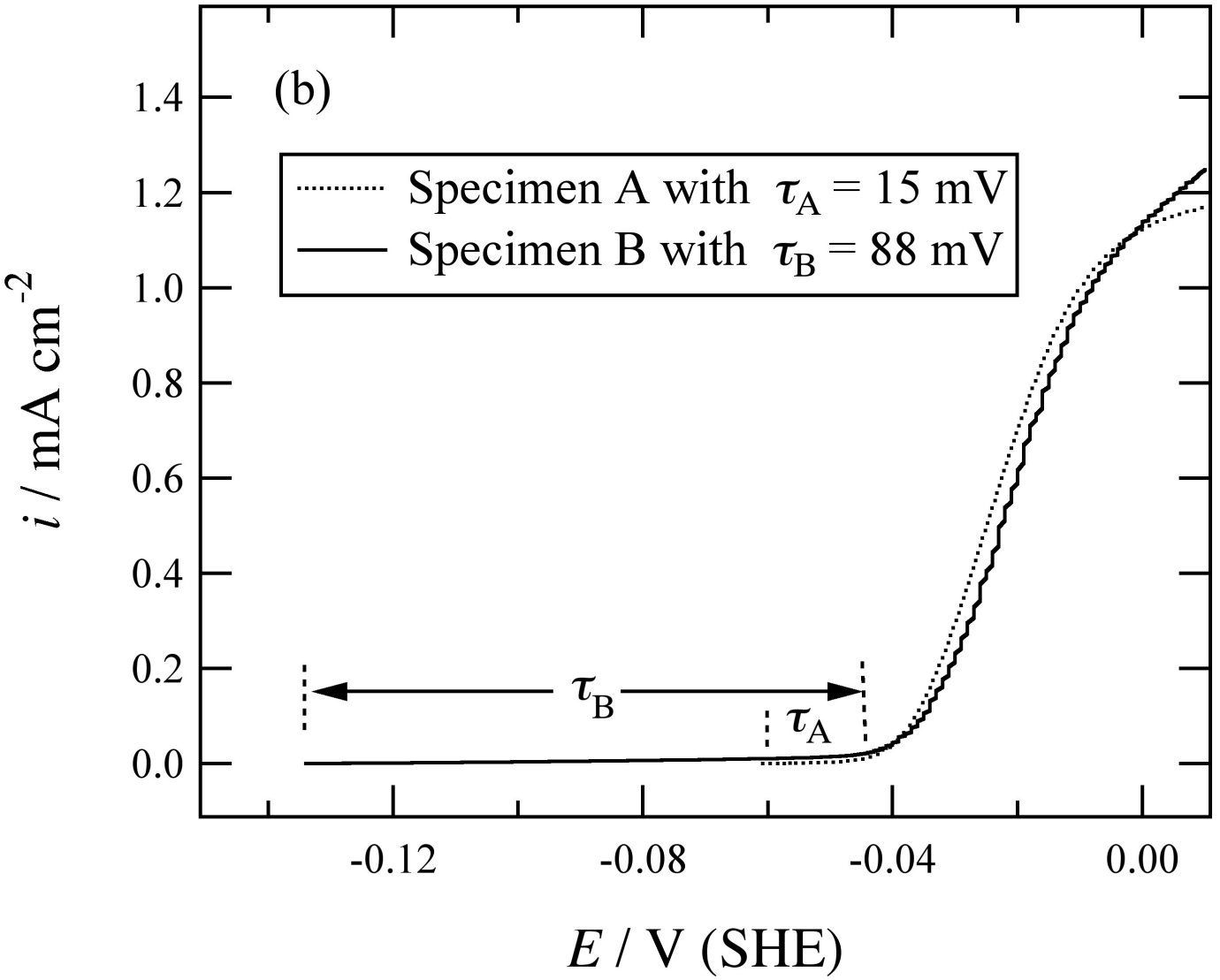
(b)
Specimen A with τ_A = 15 mV
Specimen B with τ_B = 88 mV
τ_B
τ_A
1.4
1.2
1.0
0.8
0.6
0.4
0.2
0.0
-0.12
-0.08
-0.04
0.00
i / mA cm^{-2}
E / V (SHE)

Figure 3b

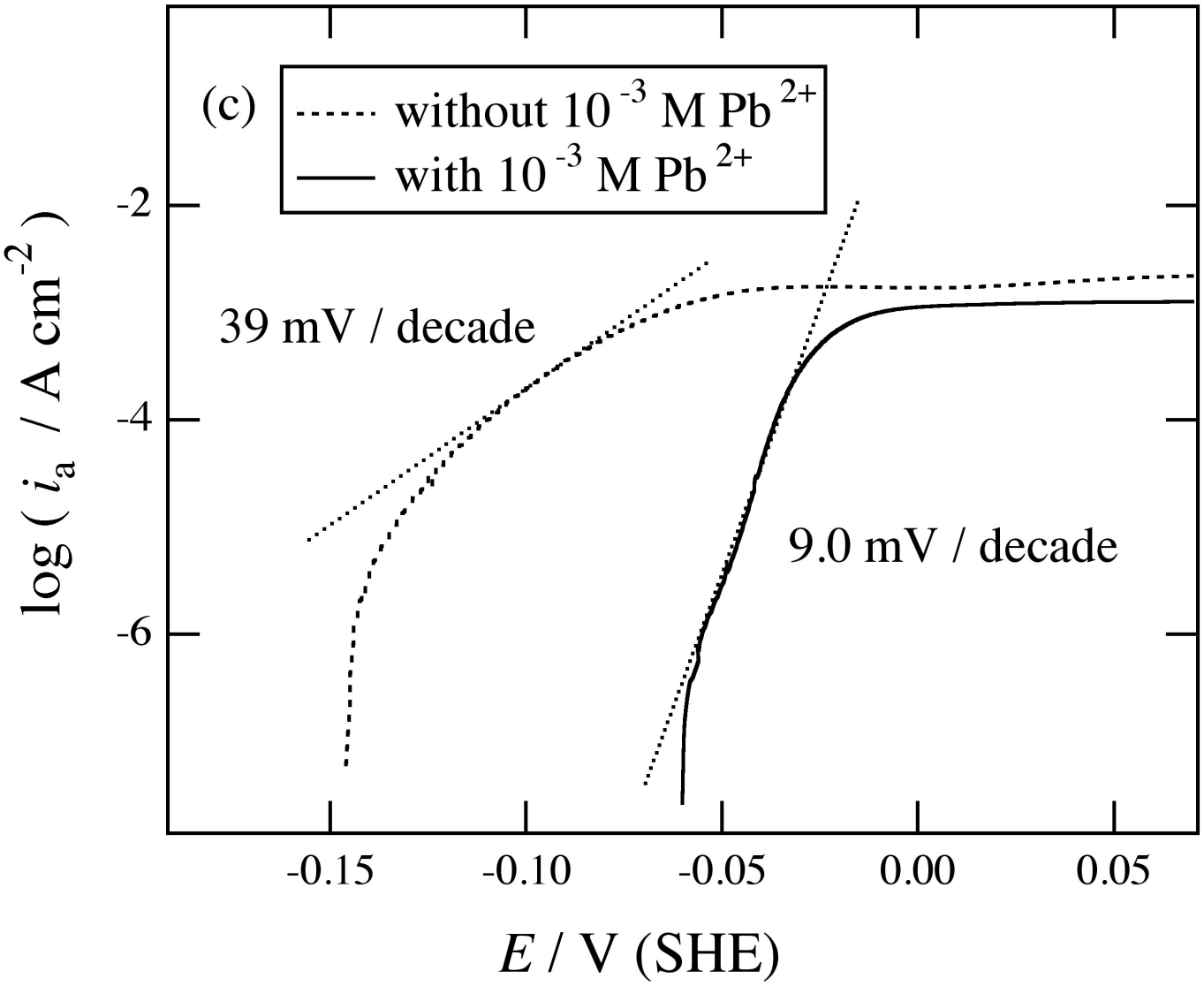
(c)
without 10 -3 M Pb 2+
with 10 -3 M Pb 2+
39 mV / decade
9.0 mV / decade
log (i_a / A cm^{-2})
-2
-4
-6
-0.15
-0.10
-0.05
0.00
0.05
E / V (SHE)

Figure 3c

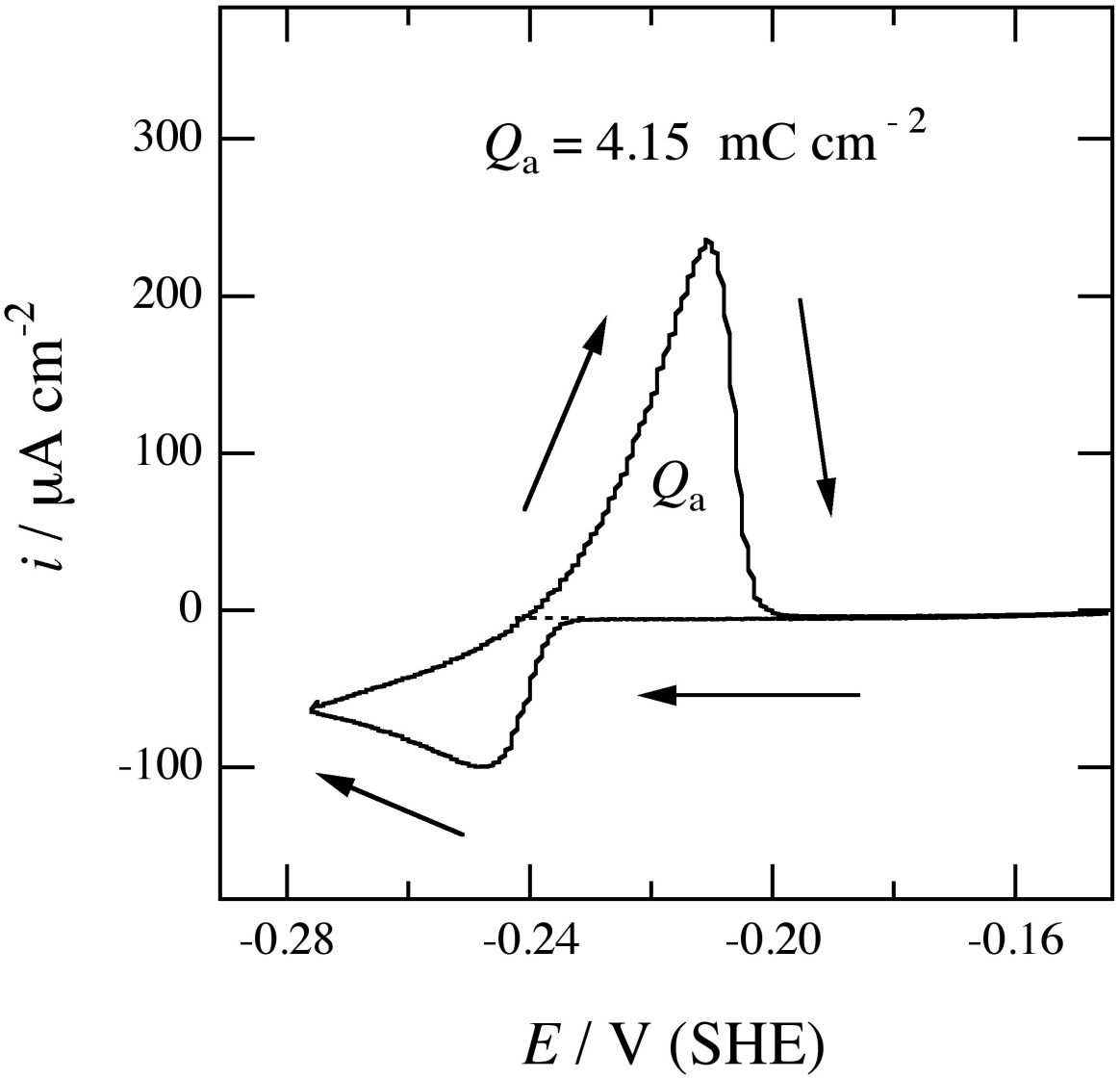

Figure 4

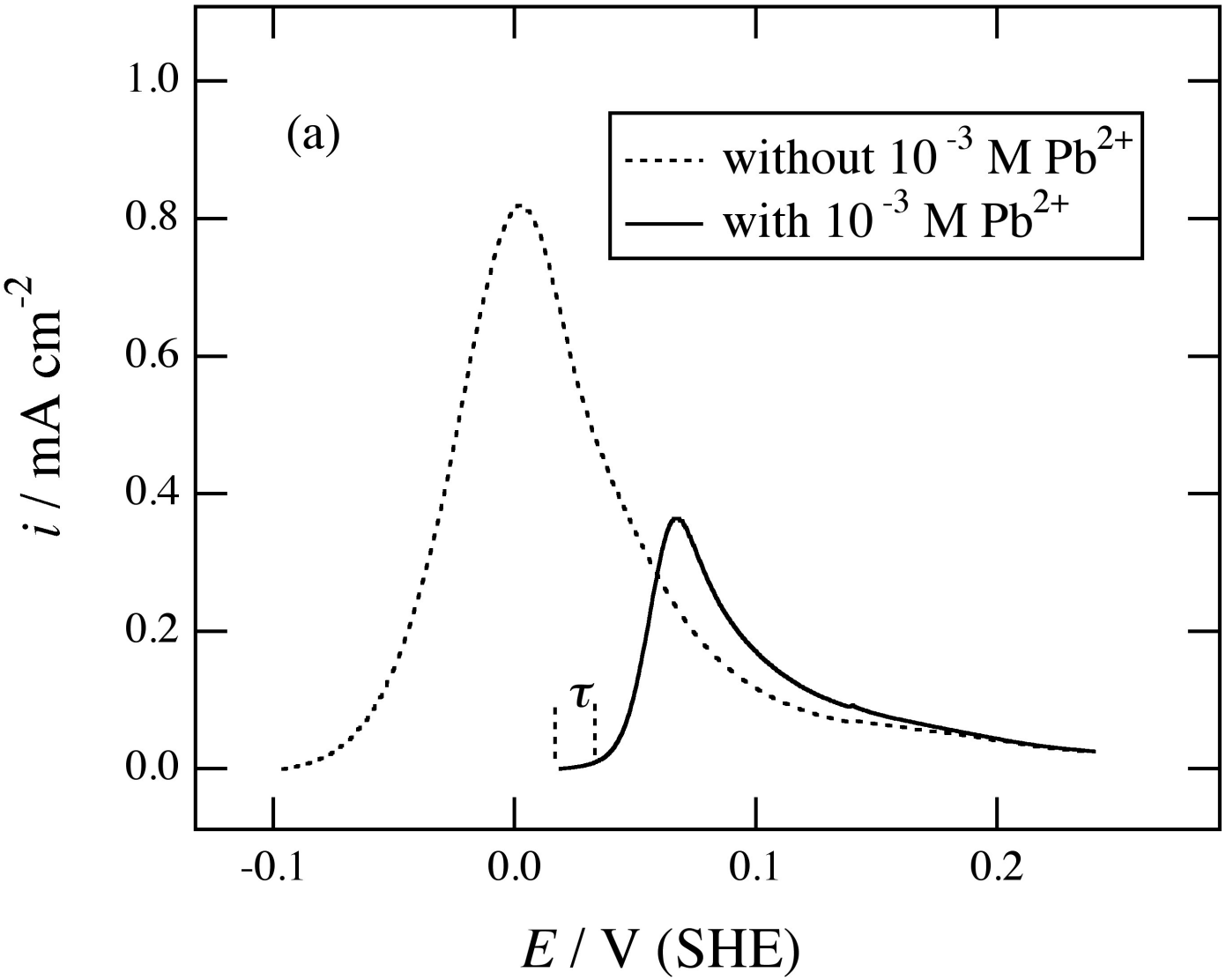
(a)
without 10 -3 M Pb2+
with 10 -3 M Pb2+
τ
i / mA cm-2
E / V (SHE)
1.0
0.8
0.6
0.4
0.2
0.0
-0.1
0.0
0.1
0.2

Figure 5a

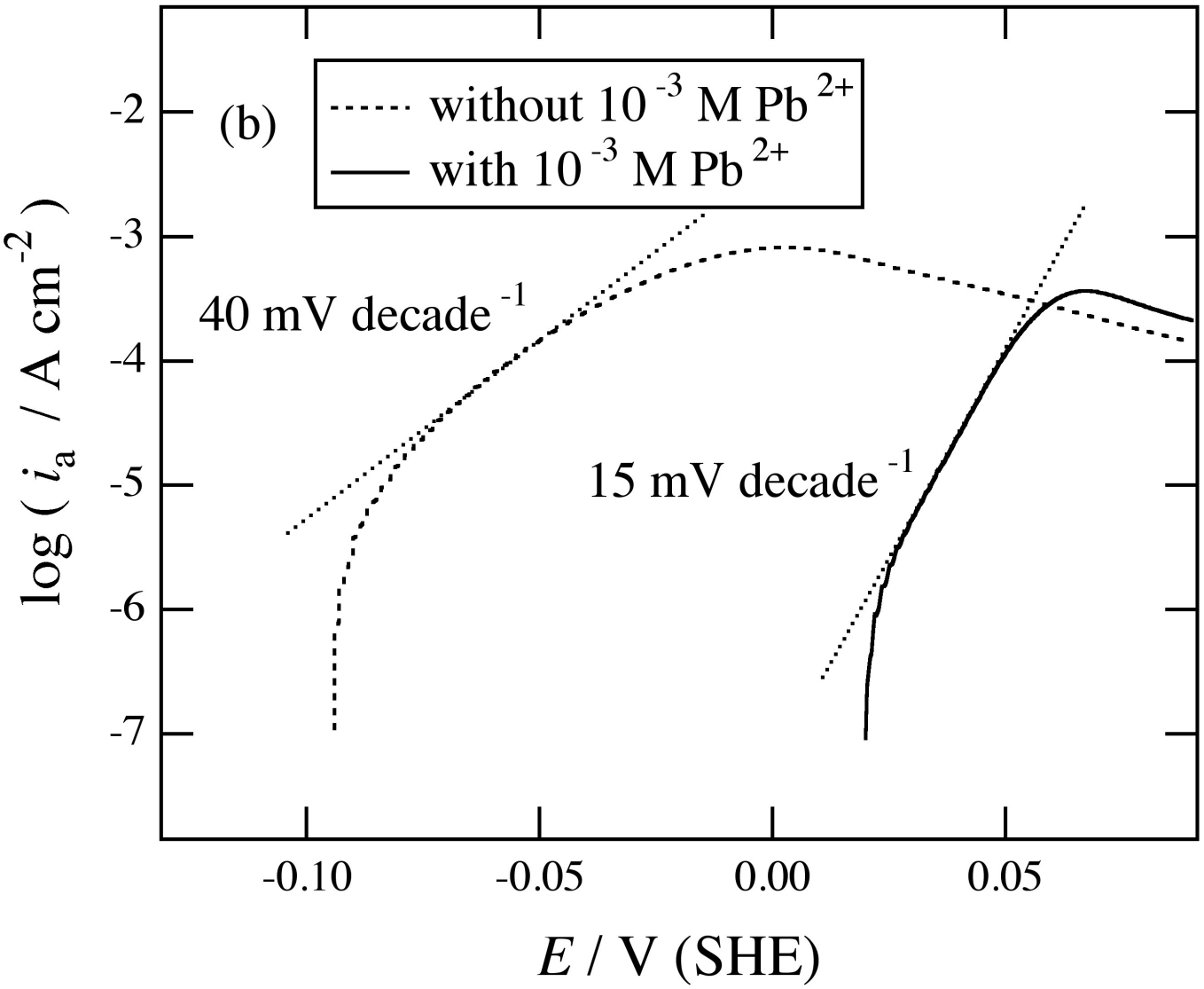
(b)
without 10 -3 M Pb 2+
with 10 -3 M Pb 2+
40 mV decade -1
15 mV decade -1
log (i a / A cm -2)
-2
-3
-4
-5
-6
-7
-0.10
-0.05
0.00
0.05
E / V (SHE)

Figure 5b

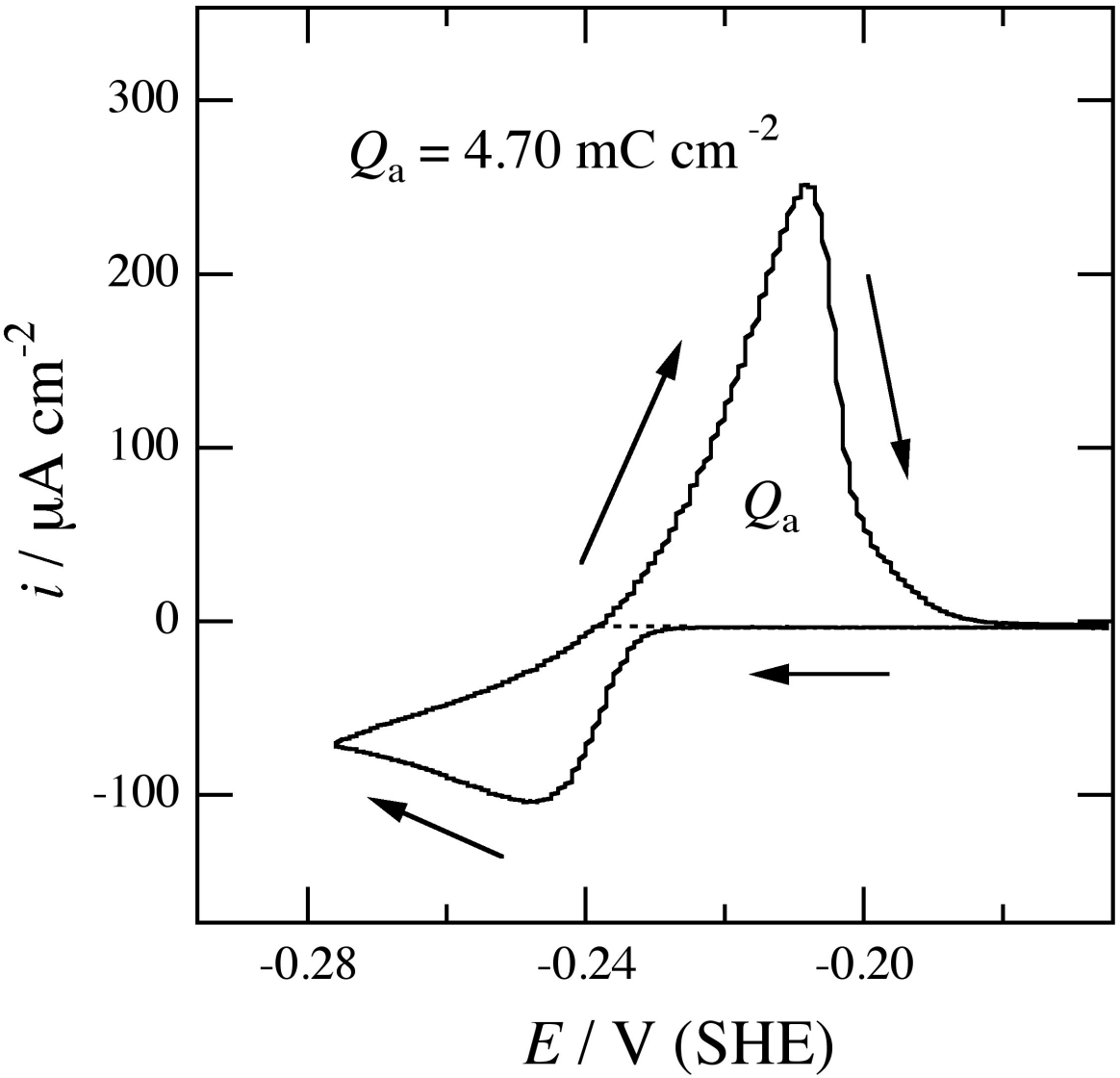

Figure 6

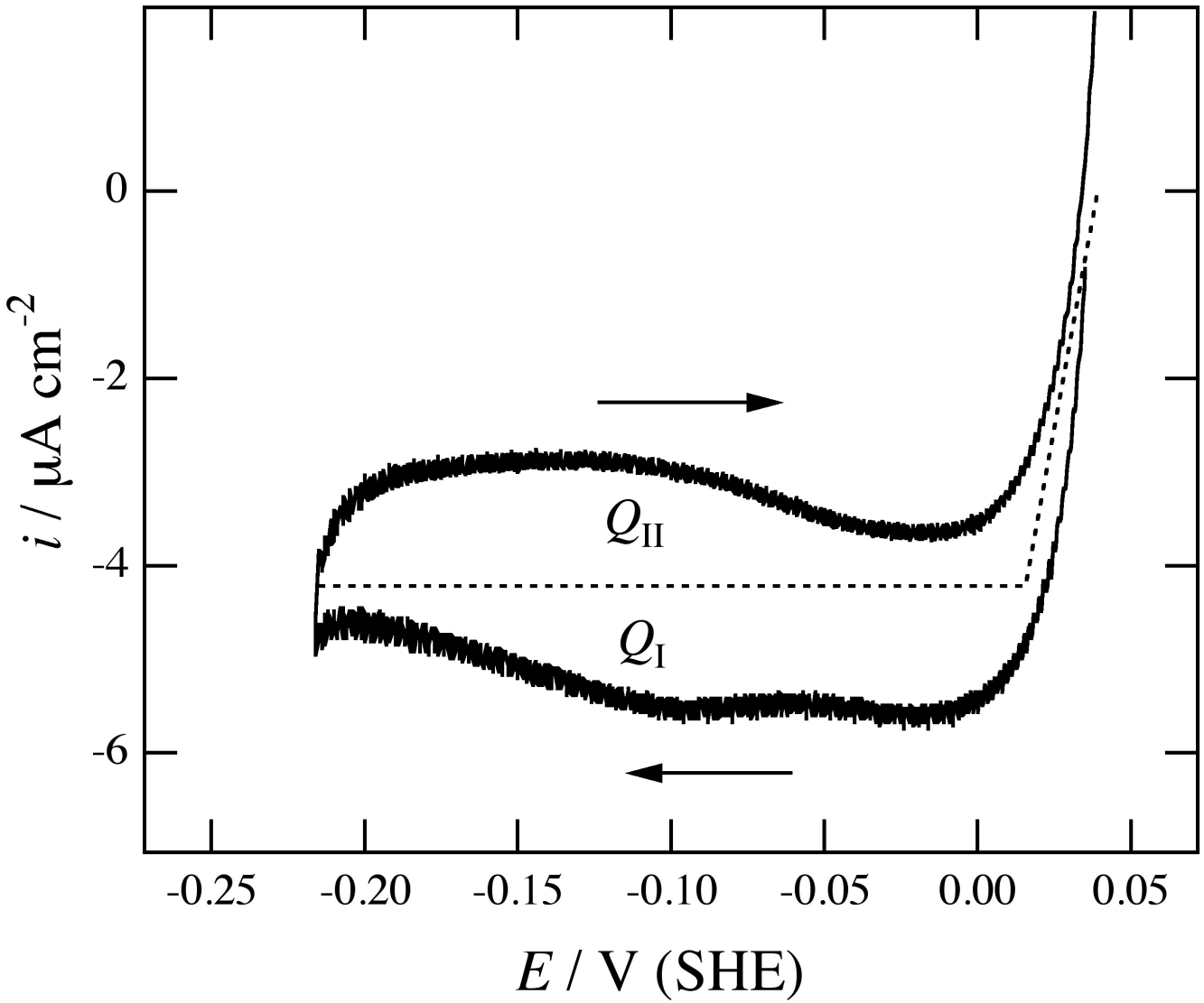

Figure 7

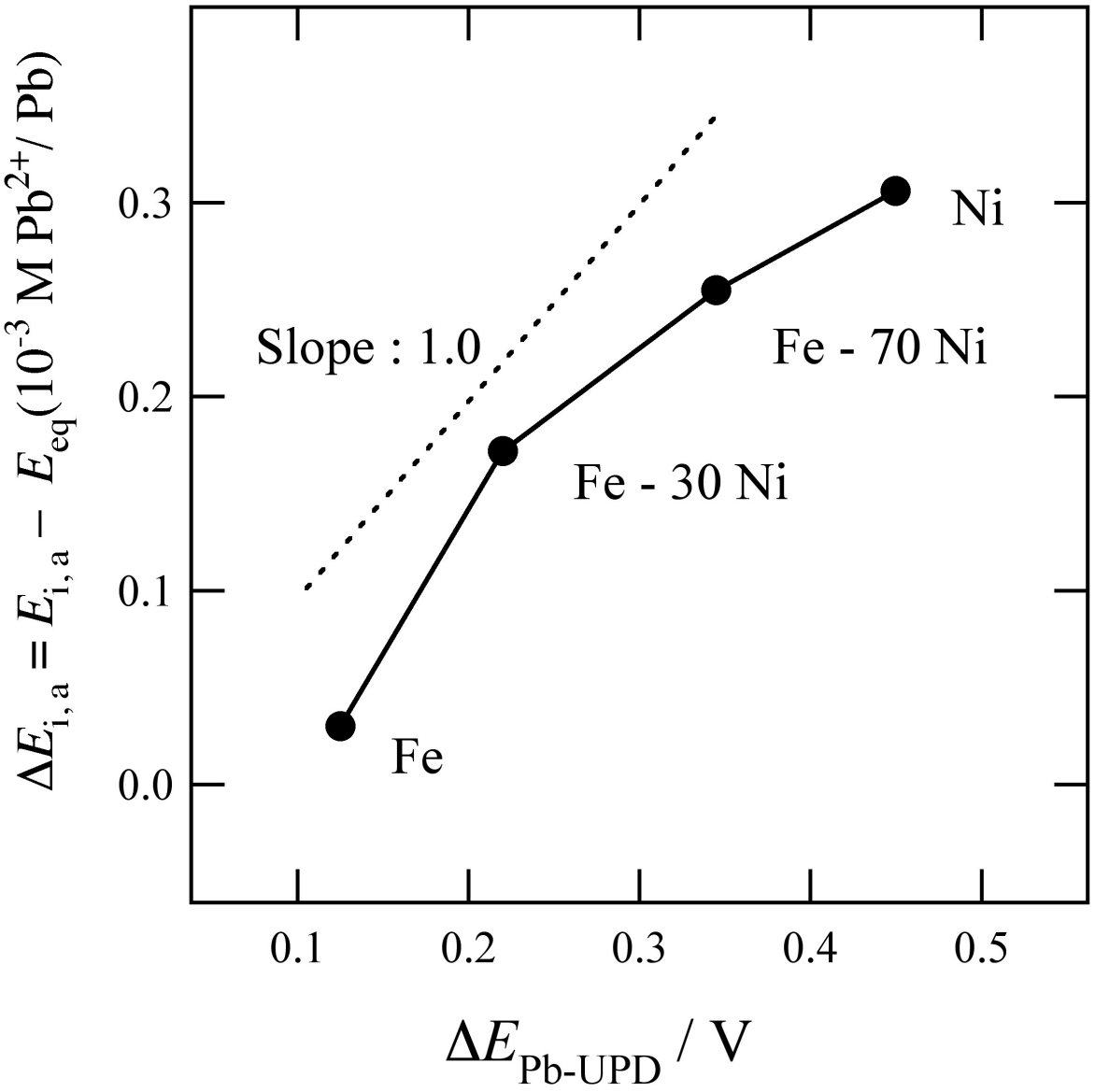
$\Delta E_{i,a} \equiv E_{i,a} - E_{eq}(10^{-3}$ M Pb^{2+}/ Pb)
0.3
0.2
0.1
0.0
Slope : 1.0
Ni
Fe - 70 Ni
Fe - 30 Ni
Fe
0.1
0.2
0.3
0.4
0.5
$\Delta E_{Pb\text{-}UPD}$ / V

Figure 8